ACS APPLIED POLYMER MATERIALS

pubs.acs.org/acsapm Article

Thermally Activated Shear Stiffening in Polymer-Grafted Nanoparticle Composites for High-Temperature Adhesives

Di Wu, Yang Ge, Ruhao Li, Yi Feng, and Pinar Akcora*

Cite This: ACS Appl. Polym. Mater. 2022, 4, 2819−2827 Read Online

ACCESS | Metrics & More | Article Recommendations | Supporting Information

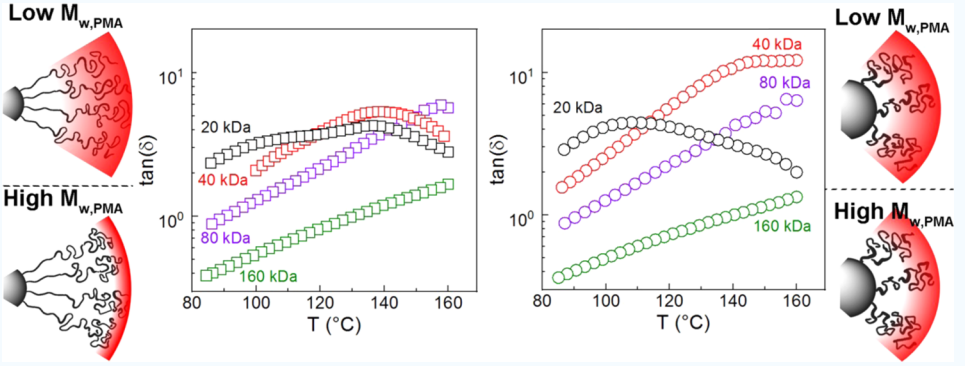

ABSTRACT: Thermally activated shear stiffening viscoelastic fluid can help to improve the performance of viscoelastic dampers and high-temperature adhesives. Polymer nanocomposites with heterogeneous interphases are applied to design such adaptive materials. In this work, shear stiffening in polymer-grafted nanoparticle composites is investigated. We report the linear rheological responses of grafted particle composites before and after large-amplitude oscillatory shear application. We found that interfacial mixing of short grafts with chemically different long matrix chains led to the enhancement of plateau moduli and terminal relaxations, unlike with the long grafts. Moreover, we showed that the elastic modulus of grafted chains was enhanced upon deformation through inter-diffusion and entanglements of interfacial layers with the short matrix chains in both grafted systems. These results suggest that dynamic coupling between chemically different polymers away from nanoparticle surfaces is a design strategy to achieve the thermally stiffening behavior in polymer nanocomposites.

KEYWORDS: *polymer nanocomposites, grafted nanoparticles, interphases, adsorption, deformation, rheology, adaptive, shear stiffening*

INTRODUCTION

The structure, dynamic behavior of polymers, and particle dispersion determine the mechanical properties of nanocomposites. Rheological studies have largely investigated the role of polymer bridging,[1,2] bound polymer chains,[3] particle dispersion,[4−6] and particle loading[7,8] on reinforcement of nanocomposites. Interfacial chain mobility gradient, chain relaxations, and particle dynamics have been extensively explored to understand the dynamic response of polymer nanocomposites.[9−17] The viscoelastic properties of composites consisting of one homopolymer type are governed by chain conformations,[18,19] adsorption,[18,20,21] and confinement of chains[22−25] in the vicinity of nanoparticles.

Chain dynamics around nanoparticles govern the rheological properties of polymer nanocomposites. The immobilized bound layers have been studied extensively for the bare particle systems. However, there is still scarce knowledge for grafted particles, particularly for their composites, where the interfacial polymer layers consist of chemically different grafted and matrix chains. We proposed in our previous experiments that chain dynamics around nanoparticles can be tuned by mixing two polymers with different glass transition temperatures, which in turn influences the mechanical properties of nanocomposites at high temperatures.[18,20,21,26−28] This study aims to explore this thermal-stiffening effect for architectural polymers simply by using polymer-grafted nanoparticle composites. The thermal-stiffening effect can be used in viscoelastic dampers,[29,30] which require high modulus and high viscosity under the oscillating shear application. Another potential application of thermal-stiffening in polymer composites is the high-temperature adhesives.[31] The energy dissipation through chain binding on particles and chain mobility provides unique mechanical properties to the

Received: January 17, 2022
Accepted: March 1, 2022
Published: March 14, 2022

uncrosslinked and grafted nanoparticle composite adhesives. Furthermore, the composite can be responsive to magnetic field-induced internal heating with the addition of magnetic nanoparticles.[27]

Dynamic asymmetry in miscible blends as in poly(ethylene oxide) (PEO)−poly(methyl methacrylate) (PMMA) blend has been studied to optimize their mechanical and conducting properties.[32−37] This complex dynamic heterogeneity governs the linear viscoelastic behavior of polymer nanocomposites. Several factors such as chain length,[21] rigidity,[18,20,38] chain architecture,[18] and glass transition temperature differences[21] control the mixing as well as the packing and entanglement density of chains within the interfacial layers. In previous studies, we studied the role of chain rigidity on the reinforcement of PEO and poly(methyl acrylate) (PMA) nanocomposites.[20,27,39] We showed that particles adsorbed with less rigid polymers improved the entanglement density of PMA matrix chains.[20] Consequently, the dense interphase layer slowed down the matrix polymer dynamics and the particle diffusion.[20] This interphase layer has been investigated for two different composite systems, where grafted and matrix chains were chemically identical and different.[18,40] In the chemically identical system, large-amplitude oscillatory shear was applied to enhance the mixing of matrix chains into the grafts and to orient the particles in the direction of shear flow.[40] In the chemically different system, the denser entanglements were achieved with the adsorbed particles compared to the grafted particles under deformation.[18]

To study the effect of different chain conformations of grafts, it would be ideal to measure the rheological properties of particles with the same graft density at varying graft lengths. We have shown that PMMA-adsorbed SiO_2 nanoparticles, which were dispersed in PEO, exhibited stiffening behavior as temperature sweeps around glass transition temperature (T_g) of PMMA.[28] This unusual reversible thermal-stiffening response of PEO nanocomposites was attributed to the dynamics of polymer chains within the interphases of PEO matrix and PMMA-adsorbed chains near nanoparticles.[28,41] Rouse dynamics of PEO chains was measured in neutron spin-echo experiments for the bare and PMMA-adsorbed SiO_2 containing PEO composites. At temperatures lower than the T_g of PMMA, the PEO chains were found to disentangle around glassy PMMA, and the reptation tube size of PEO increased.[41] At temperatures higher than the T_g of PMMA, reptation tube diameter was unchanged, revealing the dynamic coupling process between highly entangled adsorbed and matrix chains.

The mixing of chains in the interfacial region is strongly dependent on the matrix chain length. Within this interfacial layer, matrix chains were entangled and trapped in the loops of chemically different adsorbed chains. In polymer-adsorbed nanoparticles, it is not easy to control the adsorption of polymer blends on nanoparticles. Grafted particles serve well for this purpose since we control the amount of grafted chains on particles and conformations by changing graft length and density. We hypothesize that thermal-stiffening response in grafted particle systems can be achieved at intermediate graft density, and the inter-mixing of high-T_g polymer grafts (PMMA) with low-T_g matrix polymer (PMA) becomes possible under large-amplitude oscillatory shear. In this work, the viscoelastic data of composites with two different graft lengths and at different matrix chain lengths are presented to provide a deeper understanding of thermal-stiffening and reinforcement in composites with dynamic heterogeneities.

MATERIALS AND METHODS

Polymerization of Methyl Acrylate. Poly(methyl acrylate) (PMA) at 20, 80, and 160 kDa was synthesized by reversible addition-fragmentation chain transfer (RAFT) polymerization. 0.010 g of chain transfer agent (CTA) 2-cyano-2-propyl benzodithioate, 0.016 g of initiator azobisisobutyronitrile (AIBN), and 10 mL methyl acrylate (MA) monomer were dissolved in 10 mL of THF and degassed by freeze−pump−thaw and reacted at 60 °C for 3 days. PMA was precipitated in methanol and was then dried under vacuum at 130 °C for 7 days. Molecular weights of 3 batches of PMA homopolymers were estimated using the scaling relationship between the degree of polymerization (N) and the terminal relaxation time (τ_t) for polymers 1 and 2: $N_1/N_2 \sim (\tau_{t1}/\tau_{t2})^{1/3}$. τ_{t1}, τ_{t2} were measured in oscillatory shear experiments at 35 °C (Figure S1). The known molecular weight of PMA (40 kDa, purchased from Sigma-Aldrich), was used for polymer 2. . The frequency dependence of complex viscosities for different PMA composites is shown in Figure S2. Complex viscosities of synthesized PMA homopolymers at different molecular weights are shown in Figure S3.

PMMA-Adsorbed Fe_3O_4 Nanoparticles. Iron oxide (Fe_3O_4) nanoparticles (15 ± 3 nm in diameter) purchased from Rosecreek Technologies Inc. were surface-modified with (3-aminopropyl)-triethoxysilane (APTES, 99%, Sigma-Aldrich), following the procedures reported in our previous work.[27] The modified particles were mixed with 143 kDa PMMA (PDI: 1.3) in acetonitrile (15 mg/mL) and then sonicated for 10 min, followed by 30 min of rigorous stirring. PMMA-adsorbed Fe_3O_4 nanoparticles were collected by centrifugaration and washed with the corresponding solvent several times to remove all free polymers. The collected particles were dried under vacuum at room temperature and then mixed with PMA (40 kDa Sigma-Aldrich) in acetonitrile.

PMMA-Grafted Fe_3O_4 Nanoparticles. 120 mg amine-functionalized Fe_3O_4 nanoparticles were dissolved in 100 mL of *N*,*N*-dimethylformamide (DMF), Pharmco, reagent grade ACS. Then, 2 mL of 2,2′,2″-triaminotriethylamine (TAEA), Aldrich, 96% and 2 mL of α-bromoisobutyryl bromide, Aldrich, 98% (BiBB) were added dropwise into the solution and allowed to react at 60 °C for 12 h. The initiator-attached Fe_3O_4 nanoparticles were collected by centrifuging and washed three times with acetone to remove the unattached initiator. After drying at room temperature, 40 mg product particles in 30 mL of toluene/acetone (1:1) mixture and 10 mL of distillated methyl methacrylate (MMA) monomer, Acros Organics, 99% were mixed. Copper (99.99%) wire was used as the catalyst. Then, 1 mL of *N*,*N*,*N*′,*N*″,*N*″-pentamethyldiethylenetriamine (PMDETA), Aldrich, 99% was added, and the reaction time was controlled to achieve different graft lengths. PMMA-grafted Fe_3O_4 nanoparticles were centrifuged, washed four times in toluene, and dried under vacuum at room temperature. Fourier transform infrared spectroscopy (FTIR), Bruker Optics Tensor 27 data after each step of particle functionalization is presented in Figure S4.

Gel Permeation Chromatography. The weight-averaged molecular masses of grafted PMMA chains were measured using a gel permeation chromatography-light scattering (GPC/LS) instrument after etching the particles, as shown in Figure S5a,b. The GPC/LS system in our laboratory is equipped with a VARIAN PL 5.0 μm Mixed−C gel column (7.5 mm ID), a light scattering detector (miniDawn, Wyatt Technology), and a refractive index (RI) detector (Optilab rEX, Wyatt).

Thermogravimetric Analysis. The amount of adsorbed and grafted polymer on nanoparticles was determined by TA Q50 thermogravimetric analyzer (TGA). Samples were preheated at 150 °C for 20 min and then heated to 550 °C at a 5 °C/min heating rate. TGA curves for polymer-adsorbed or grafted Fe_3O_4 nanoparticles are shown in Figure S5c. The grafting density was estimated from $\sigma = a\frac{\rho R}{3M}N_A$, where a is the mass ratio of grafted (or adsorbed) chains and nanoparticles obtained from TGA data, ρ is the density of Fe_3O_4

https://doi.org/10.1021/acsapm.2c00097
ACS Appl. Polym. Mater. 2022, 4, 2819−2827

(5.2 g/cm^3), M is the molecular weight of adsorbed chains, and R is the radius of Fe_3O_4 nanoparticles (7.5 nm).

Rheology Experiments. Linear viscoelastic data of polymer nanocomposite melts were measured in ARES-G2 strain-controlled rheometer using 8-mm parallel plates. Time-temperature superposition (TTS) curves were obtained at 35, 55, 85, and 140 °C, and the frequency range was 0.1−100 rad/s for each temperature. The reference temperature of 35 °C was above the T_g of PMA (15 °C). The rubbery plateau modulus of samples is determined by finding the G' at the frequency at which the tan(δ) reaches a minimum, as illustrated in Figure S6.

RESULTS AND DISCUSSION

39 and 148 kDa PMMA-grafted at the same grafting density (0.045 chains/nm^2) on Fe_3O_4 (15 nm in diameter) nanoparticles were synthesized and mixed with PMA at 20, 40, 80, and 160 kDa molecular weights in solution. PMMA adsorption and grafting procedures on nanoparticles are described in the Experimental Section. These modified particles were mixed with PMA (10 mg/mL) acetonitrile solution, stirred vigorously for 1 h and sonicated for 30 min, and then solution-cast in Teflon cups. After complete solvent evaporation in air, composite films were annealed in a vacuum oven at 130 °C for 3 days before use. The particle core loading was 15 wt % in all samples. Molecular weights of each component (matrix, grafted, and adsorbed chains) are given in Table 1. Composite disks 1 mm thick and 8 mm in diameter were prepared with a home-built molding fixture with vacuum line for small-angle X-ray scattering (SAXS) and rheological tests. SAXS experiments were run in Ganesha, SAXSLAB instrument at Columbia University.

Table 1. Synthesized PMA Composite Samples Differ in Their Matrix and Grafted Chain Lengths. Molecular Weights of PMA Homopolymer Matrices, PMMA Adsorbed on Particles, PMMA-Grafted on Particles, and Grafting Densities Are Listed.

PMA matrix molecular weight (kDa)	nanoparticles	chain density (chains/nm^2)
40	143 kDa PMMA-adsorbed Fe_3O_4	0.019
20, 40, 80, 160	39 kDa PMMA-grafted Fe_3O_4	0.045
20, 40, 80, 160	148 kDa PMMA-grafted Fe_3O_4	0.045

Particle dispersion of PMMA-grafted Fe_3O_4 nanoparticles in different molecular weights of PMA matrices was characterized in small-angle X-ray scattering (SAXS) (Figure 1). We applied a two-level unified function, but it did not fit well at low q (Figure S7). The three-level unified function was then applied to obtain particle structure sizes (R_{g1}, R_{g2}, R_{g3}) with corresponding G prefactors and fractal dimensions (P exponents) (Table S1). The primary particle size (R) was calculated as 6.5 nm using $R = \sqrt{\frac{5}{3}} R_{g1}$. R_{g2} and R_{g3} show the average sizes of the second and third level structures of particle networks with P values between 4 and 5, describing a diffusive interphase.[42] R_{g3} is introduced to fit the low-q region of the data, and it has a larger value (30−40 nm) than R_{g2} (10−20 nm) for all samples. In both long (148 kDa) and short (39 kDa) graft systems, the aggregate sizes (R_{g2} and R_{g3}) decrease with increasing molecular weights of the matrix polymer. The entropic repulsion of long chains reduces the aggregate sizes. In the 20 kDa PMA matrix, 148 kDa PMMA-grafted sample shows larger aggregation sizes than 39 kDa grafted sample. This result indicates that the particle−particle interactions become stronger with the long-grafted PMMA chains in short matrix chains. A simulation work on grafted nanoparticles without any free chains supported this result.[43] The ratio among the G parameter in the three-level Unified Model refers to the relative concentration population of aggregates with sizes of R_{gi} (Table S1).

PMA is not easy to cryomicrotome and presented lots of artifacts during sample preparation. Since our samples have dynamic heterogeneity around nanoparticles, adhesion force maps allow imaging stiff domains with glassy PMMA chains in bulk samples. We tested short and long PMMA-grafted nanoparticles in the 20 kDa PMA matrix. Sample disks used in rheology experiments were gently flattened at 60 °C to create a smooth surface and then tested in adhesion force mapping mode (Peakforce QNM) of the atomic force microscopy (AFM) of Bruker BioScope Resolve High-Resolution BioAFM with a Nikon Ti-2 fluorescent microscope. Note that PMMA is glassy, and the PMA matrix is very soft at 60 °C. Dark areas have the lowest adhesion forces; thus, they represent stiff regions of the long-graft (148 kDa) sample, and grafted particles were arranged anisotropically, forming ∼300 nm wide, stiff structures (Figure 2**a**). The short-graft (39 kDa) sample has much larger anisotropic aggregates from ∼200 to ∼1000 nm wide, as shown in Figure 2**b**. The scan area was

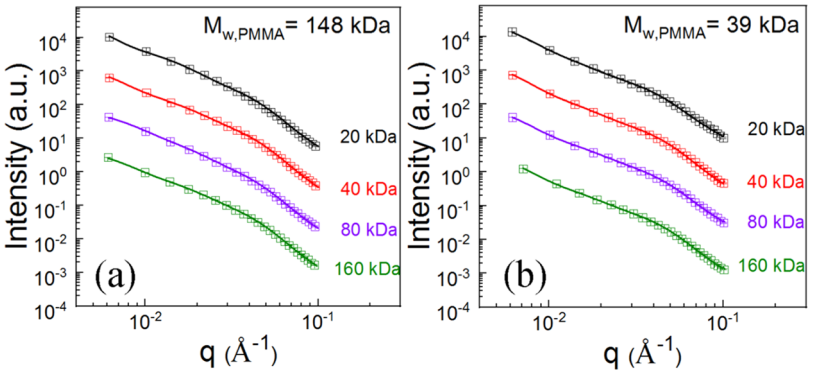

Figure 1. SAXS data for PMA (20, 40, 80, 160 kDa) composites with (**a**) PMMA (148 kDa)-grafted and (**b**) PMMA (39 kDa)-grafted Fe_3O_4 nanoparticles. Lines represent the three-level unified function fits. Data series were vertically shifted for clarity. Particle core loading is 15 wt % in all samples.

https://doi.org/10.1021/acsapm.2c00097
ACS Appl. Polym. Mater. 2022, 4, 2819−2827

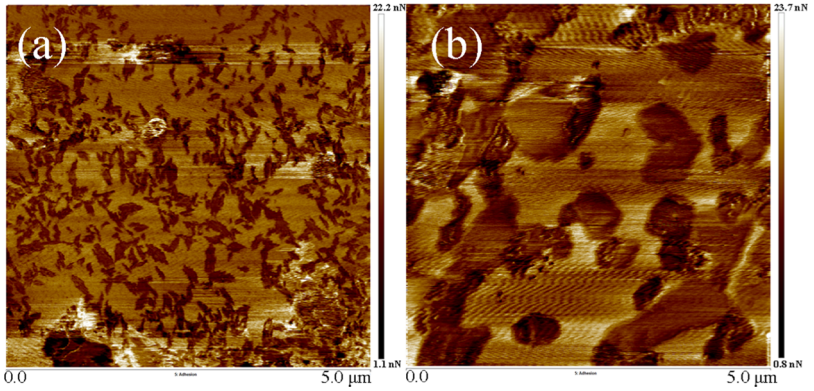

Figure 2. Adhesion force maps on bulk PMA composites for (**a**) 148 kDa PMMA-grafted Fe_3O_4 and (**b**) 39 kDa PMMA-grafted Fe_3O_4 in 20 kDa PMA at 60 °C.

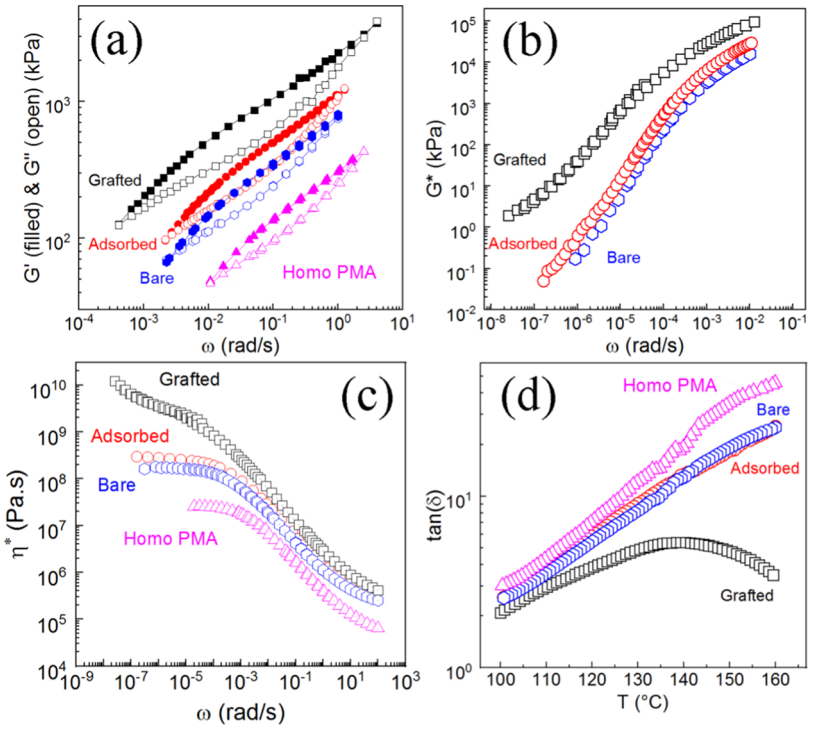

Figure 3. Rheological responses of bare, PMMA-grafted, and PMMA-adsorbed nanoparticle composites. (**a**) Linear viscoelastic data; (**b**) complex moduli (G^*); and (**c**) complex viscosities (η^*) of PMA (40 kDa) nanocomposites of bare Fe_3O_4, PMMA (143 kDa, 0.019 chains/nm^2)-adsorbed, and PMMA (148 kDa, 0.045 chains/nm^2)-grafted Fe_3O_4 particles, measured at 35 °C. (**d**) Loss tangent, tan(δ), data during temperature sweep experiments at ω = 5 rad/s, γ = 15%. Particle core loading is 15 wt %, and the molecular weight of PMA is 40 kDa in all composites.

focused on a 5 μm × 5 μm region. Adhesion force maps measured at lower magnification (25 μm × 25 μm) are shown in Figure S8. These data show that longer grafts can aid the phase stability of particles more than the shorter ones and the short-graft chains create more aggregated stiff regions in bulk composites. This observation matches the SAXS fitting results, which indicate that long-graft particles form smaller structures (R_{g2} and R_{g3}) than short grafts.

Interfacial layers of the grafted and adsorbed samples differ in chain conformations and entanglements. Thus, different hydrodynamic contributions and entanglements in these samples contribute to their reinforcements. The small-amplitude oscillatory shear (SAOS) data in Figure 3**a** shows that grafted and adsorbed particles reinforce the composite more than the bare particles. The viscoelastic modulus is enhanced by an order of magnitude with the grafted system compared to the bare composite, and the rubbery plateau modulus of grafted particles is measured to be higher than the adsorbed particles in the same matrix polymer as seen in complex modulus (G^*) versus frequency data (Figure 3**b**). The hydrodynamic contribution of adsorbed, bare, and grafted particles at constant volume fraction (ϕ = 0.05) is evaluated by the viscosity enhancement $\left(\frac{\eta_{PNC}}{\eta_{matrix}}\right)$ as predicted by the Einstein equation,[44] $\left(\frac{\eta_{PNC}}{\eta_{matrix}}\right) = 1 + 2.5\phi = 1.125$. The viscosity, however, was enhanced by 6.4 times for the bare composite (η_{PNC}, estimated using the viscosity data in Figure S2b) compared to the pure matrix zero shear viscosity (η_{matrix}), and by 10 times for the adsorbed samples as presented in Figure 3**c**. For the grafted composite, a modified Einstein equation[7] is used:

https://doi.org/10.1021/acsapm.2c00097
ACS Appl. Polym. Mater. 2022, 4, 2819−2827

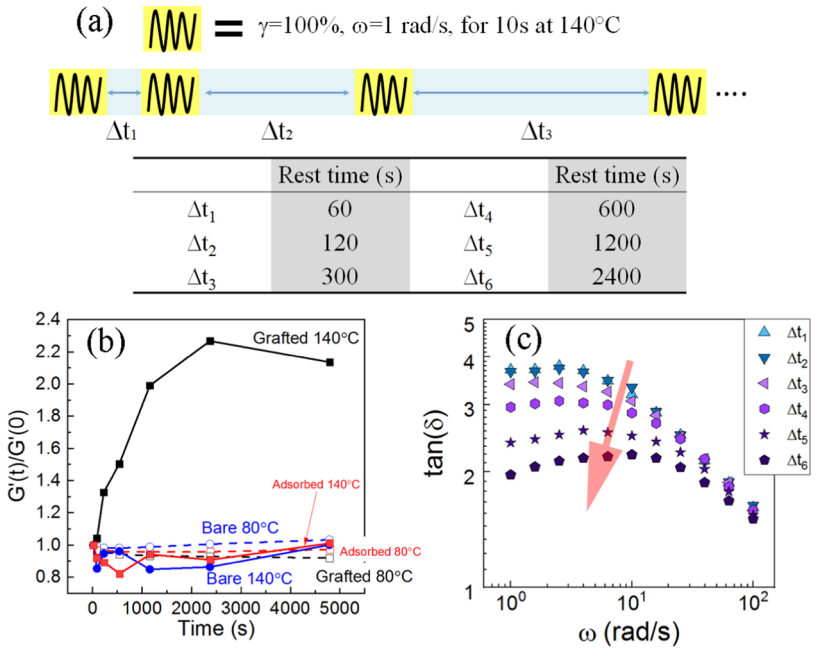

	Rest time (s)		Rest time (s)
Δt_1	60	Δt_4	600
Δt_2	120	Δt_5	1200
Δt_3	300	Δt_6	2400

Figure 4. (**a**) Shear-rest experiment protocol with increasing rest times (Δt_n). (**b**) Storage modulus normalized by the modulus of undeformed state at t = 0 is plotted for different rest times measured at 140 and 80 °C for bare and grafted composites. (**c**) Loss tangent of the grafted composite obtained in linear experiments conducted at γ = 20% and 140 °C after each large deformation.

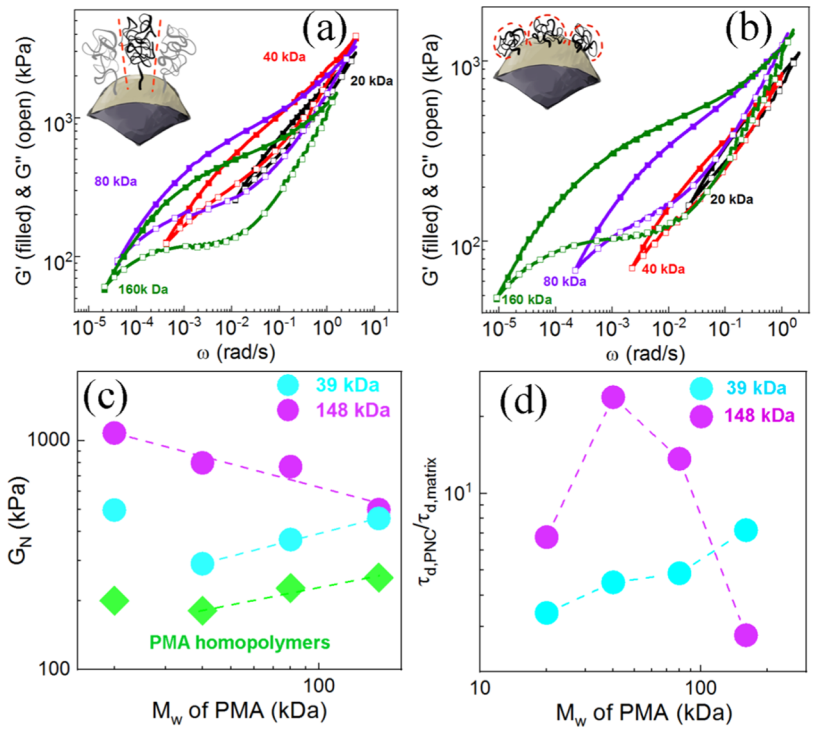

Figure 5. Effect of graft and matrix molecular weights on viscoelastic responses of PMA nanocomposites. Linear viscoelastic data at rubber plateau of nanocomposites at different PMA matrix molecular weights with (**a**) 148 kDa PMMA-grafted nanoparticles and (**b**) 39 kDa PMMA-grafted nanoparticles. (**c**) Rubbery plateau modulus (G_N) of composites with different PMA matrix molecular weights. (**d**) Terminal relaxation time of a grafted particle composite normalized by that of the PMA matrix for different molecular weights (20, 40, 80, and 160 kDa). The terminal relaxation times are determined using the crossovers at the lower frequency in panels (**a**) and (**b**).

$\frac{\eta_{PNC}}{\eta_{matrix}} = 1 + 2.5\phi\left(1 + \frac{4R_g}{D}\right)^3$, where R_g is for the gyration radius of grafted chains on particles and D is the particle diameter. The model assumes that the thickness of the grafted brush equals $2R_g$ of the grafted chains. The R_g of PMMA chains is calculated as 10.23 nm using the equation $R_g = b\sqrt{\frac{M}{6M_{Kuhn}}}$, where the Kuhn length (b) = 1.5 nm, the Kuhn molar mass (M_{Kuhn}) = 529.4 g/mol for M = 148 kDa PMMA.[45] The modified Einstein equation gives 7.5 for $\frac{\eta_{PNC}}{\eta_{matrix}}$.

https://doi.org/10.1021/acsapm.2c00097
ACS Appl. Polym. Mater. 2022, 4, 2819−2827

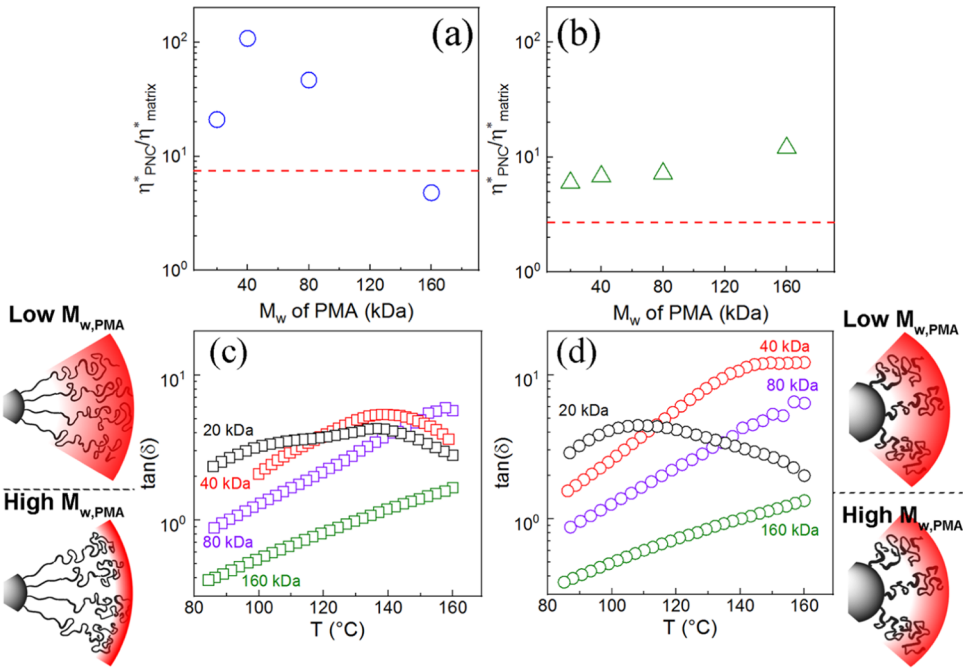

Figure 6. Effect of matrix molecular weight on viscosity enhancement in polymer nanocomposites. The normalized viscosities of (**a**) 148 kDa PMMA-grafted Fe_3O_4 and (**b**) 39 kDa grafted Fe_3O_4 nanoparticle composites in varying matrix molecular weights. The red line is the calculated viscosity from $\frac{\eta_{PNC}}{\eta_{matrix}} = 1 + 2.5\phi\left(1 + \frac{4R_g}{D}\right)^3$. The η_{PNC} values are obtained by averaging the viscosity data highlighted in Figure S2. Linear viscoelastic data from temperature sweep experiments for composites with PMA matrix molecular weights varying between 20 and 160 kDa with (**c**) 148 kDa and (**d**) 39 kDa PMMA-grafted nanoparticles at 5 rad/s frequency. The heating rate was 5 °C/min. γ was selected at 2−20% for linear response.

This predicted value is also smaller than the ratio of measured viscosities of the grafted composite and homopolymer. The composite viscosity is 100 times larger than that of homopolymer viscosity (Figure 3**c**). Thus, the reinforcement enhancement of grafted composite is attributed to the higher interfacial entanglements. A decrease in tan(δ) of grafted sample is seen at 140 °C, referring to a solid-like behavior of the composite at temperatures higher than 140 °C (Figure 3**d**). This effect is not seen in bare and adsorbed composites. The observed transition is explained by the strong dynamic coupling between PMA matrix chains and grafted PMMA chains that are mobile at temperatures above $T_{g,PMMA}$.

In attractive polymer nanocomposites, the interactions between nanofillers and polymers lead to the strong adsorption of chains and good particle dispersion. It is also known that desorption−readsorption processes on attractive nanoparticle surfaces occur at very long times and high temperatures.[46] To facilitate mixing of grafted chains away from the adsorbed chains, nonlinear oscillatory shear flows were applied, and the linear elastic modulus of bare particle PMMA composite was measured during resting.[47] The stiffening of composites during the periodic deformation process arises from the enhancement in the entanglement of chains.[47] The nonlinear network model with an additional term for the interphase has been applied to analyze the stress−strain data.[18] It was found that the interphase modulus was higher for the adsorbed-particle composites than the grafted ones, and the interphase modulus decreased as graft density increased.[18] These results showed that the interphase was more deformable in grafted systems, whereas entanglements were denser in the adsorbed system and less likely to deform. The samples in this work are at higher grafting density (0.045 chains/nm^2), and we anticipate outer regions of the brush to mix with free chains under deformation.

To investigate this deformation effect, similar shear-rest experiments were conducted on grafted, adsorbed, and bare composites at 140 and 80 °C at 100% strain and 1 rad/s frequency. Each LAOS test is followed by SAOS experiment during sample resting, as presented in Figure 4**a**. The grafted composite presented an enhanced modulus by a factor of 2.3 at 140 °C, and the recovery was like the response of adsorbed and bare composites at 80 °C (Figure 4**b**). The storage modulus $G'(t)$ normalized by the initial modulus $G'(t = 0)$ shows that the grafted sample can stiffen at high temperatures only. This is because PMA chains can penetrate and entangle with the neighbor chains easily when PMMA chains are mobile at 140 °C. Linear experiments conducted right after deformation tests show that the loss tangent of the composite decreased after many cycles of deformation (Figure 4**c**), indicating the higher elastic response within the same composite. Thus, from the shear-rest experiments, we conclude that the grafted chains are more deformable under large strain compared to the adsorbed and bare composites, which is consistent with our previous findings.[18]

SAOS data at rubber plateau region for long and short PMMA-grafted particle composites in different molecular weights of PMA matrix are shown in Figure 5**a**,**b**, respectively. The rubbery plateau modulus (G_N) of short grafts increases with matrix molecular weight, while it decreases in long grafts (Figure 5**c**). The increase in terminal relaxation times of short-graft composites with different matrix molecular weights is shown in Figure 5**d**. The terminal relaxation times normalized by the corresponding matrix homopolymer increased with the short grafts but not with the long grafts. This is attributed to

https://doi.org/10.1021/acsapm.2c00097
ACS Appl. Polym. Mater. 2022, 4, 2819−2827

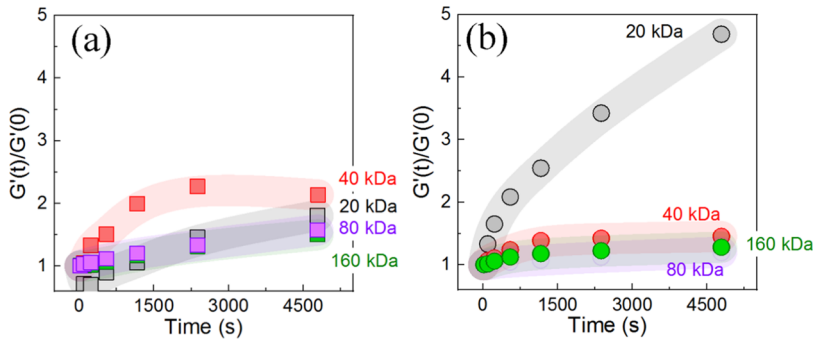

Figure 7. Normalized storage modulus measured after nonlinear deformations during long rest times for (**a**) 148 kDa and (**b**) 39 kDa PMMA-grafted nanoparticles in PMA matrices of varying molecular weights (20, 40, 80, 160 kDa). The experiments were performed at 140 °C.

the strong interactions between short grafts and matrix, and weaker interactions between long PMMA grafts with 80 and 160 kDa PMA.

Figure 6a,b show the complex viscosities of composites normalized by their matrices. In long-graft (148 kDa) samples, the viscosity enhancement is higher than the calculated viscosity. PMA matrix chains longer than the grafts create weak interfaces and reduce the complex viscosity of the composite. The viscosity of short-graft (39 kDa) composites increases with matrix molecular weights. Samples were also run in temperature sweep experiments, where the dynamics of interfacial chains is dependent on the dynamic heterogeneities of interfacial layers. Liquid-to-solid transition at 140 °C in the long-graft composite is attributed to the dynamic coupling between PMMA (148 kDa) graft and PMA matrix (20 and 40 kDa) when all chains are mobile (Figure 6**c**). Liquid-to-solid transition in the short-graft composite in the 20 kDa matrix is observed at 110 °C (Figure 6**d**). The mixing regions of short matrix chains with the grafts are illustrated with the color gradient in Figure 6. In summary, with the low molecular weight matrix chains, both graft composites present solid-like behavior but at different temperatures. This different temperature response of two composites is explained by the dynamic coupling effect of grafted chains. At temperatures higher than the T_g of the grafted polymer ($T_{g,matrix} < T_{g,graft} < T$), the mobility of the grafted chains starts to increase when the matrix chains and grafted chains become dynamically coupled.

The mixing zone of interfacial layers is further verified by applying large-amplitude oscillatory shear. The effect of the molecular weights on interfacial relaxation is explored via large deformation-rest experiments. With shear-rest experiments as described in Figure 4a, we found that the modulus enhancement in the composites with chemically heterogeneous interphases is controlled by matrix molecular weight. The normalized storage moduli versus rest time for long-graft samples are shown in Figure 7**a** and for short-graft samples in Figure 7**b**. We observed that short grafts can mix well only with short matrix chains upon deformation, and their interphases get stronger than the long grafts in the same matrix. The strongest enhancement is observed in samples with 20 kDa PMA chains, whereas no obvious increase of G' is found with other matrices.

CONCLUSIONS

In this work, we explored the effect of dynamic heterogeneities on the viscoelastic properties of polymer-grafted particle nanocomposites. To study this complex dynamic heterogeneities of interfacial layers in nanocomposites, high-T_g polymer-grafted and adsorbed nanoparticles were dispersed in a low-T_g matrix homopolymer. We showed that grafted particle composites behaved more elastic upon heating and their reinforcement effect was larger than that of the particles adsorbed with the same polymer. Long grafts exhibited a stiffening response around 140 °C as they can dynamically couple with short matrix chains. The stiffening was observed at 110 °C for the short grafts with the short matrix chains only. Notably, the interfacial entanglements enhanced for both grafted systems with short matrix chains under deformation. These findings suggest that dynamic heterogeneities govern the mixing and dynamics of low-T_g polymer nanocomposites with grafted particles. The rheological data presented herein demonstrate how the mixing (interpenetration zone) of grafted chains with the matrix can be modulated under large shear flow. We showed that the interfacial chain dynamics and interfacial chain conformations can be altered away from particle surfaces to achieve a stiffening response in polymer nanocomposites at high temperatures. This chain dynamics-controlled mixing and reinforcement in polymer nanocomposites can yield new designs for thermally activated shear stiffening viscoelastic fluid and high-temperature adhesives requiring low viscosity yet good reinforcement.

ASSOCIATED CONTENT

Supporting Information

The Supporting Information is available free of charge at https://pubs.acs.org/doi/10.1021/acsapm.2c00097.

Linear viscoelastic data of grafted particle composites and PMA homopolymers at different molecular weights; complex viscosities of composites and PMA homopolymers; FTIR data of particles; GPC data of PMMA grafts and TGA data of grafted nanoparticles; SAXS data analysis and comparison of two-level and three-level unified functions; and adhesion force maps at 25 μm × 25 μm scan area (PDF)

AUTHOR INFORMATION

Corresponding Author

Pinar Akcora − *Department of Chemical Engineering and Materials Science, Stevens Institute of Technology, Hoboken, New Jersey 07030, United States;* orcid.org/0000-0001-7853-7201; Email: pakcora@stevens.edu

https://doi.org/10.1021/acsapm.2c00097
ACS Appl. Polym. Mater. 2022, 4, 2819−2827

Authors

Di Wu − *Department of Chemical Engineering and Materials Science, Stevens Institute of Technology, Hoboken, New Jersey 07030, United States*

Yang Ge − *Department of Chemical Engineering and Materials Science, Stevens Institute of Technology, Hoboken, New Jersey 07030, United States*

Ruhao Li − *Department of Chemical Engineering and Materials Science, Stevens Institute of Technology, Hoboken, New Jersey 07030, United States*

Yi Feng − *Department of Chemical Engineering and Materials Science, Stevens Institute of Technology, Hoboken, New Jersey 07030, United States*

Complete contact information is available at: https://pubs.acs.org/10.1021/acsapm.2c00097

Author Contributions

The manuscript was written through contributions of all authors.

Funding

This material is based upon work supported by the National Science Foundation CMMI MEP program under Grant No. 1825250.

Notes

The authors declare no competing financial interest.

■ ACKNOWLEDGMENTS

The authors thank Sophia Chen and Prof. Sanat K. Kumar for SAXS experiments conducted at Columbia University.

■ REFERENCES

(1) Yavitt, B. M.; Salatto, D.; Zhou, Y.; Huang, Z.; Endoh, M.; Wiegart, L.; Bocharova, V.; Ribbe, A. E.; Sokolov, A. P.; Schweizer, K. S.; Koga, T. Collective Nanoparticle Dynamics Associated with Bridging Network Formation in Model Polymer Nanocomposites. *ACS Nano* **2021**, *15*, 11501−11513.

(2) Cheng, S.; Holt, A. P.; Wang, H.; Fan, F.; Bocharova, V.; Martin, H.; Etampawala, T.; White, B. T.; Saito, T.; Kang, N.-G.; Dadmun, M. D.; Mays, J. W.; Sokolov, A. P. Unexpected Molecular Weight Effect in Polymer Nanocomposites. *Phys. Rev. Lett.* **2016**, *116*, No. 038302.

(3) Jouault, N.; Moll, J. F.; Meng, D.; Windsor, K.; Ramcharan, S.; Kearney, C.; Kumar, S. K. Bound polymer layer in nanocomposites. *ACS Macro Lett.* **2013**, *2*, 371−374.

(4) Akcora, P.; Liu, H.; Kumar, S. K.; Moll, J.; Li, Y.; Benicewicz, B. C.; Schadler, L. S.; Acehan, D.; Panagiotopoulos, A. Z.; Pryamitsyn, V.; Ganesan, V.; Ilavsky, J.; Thiyagarajan, P.; Colby, R. H.; Douglas, J. F. Anisotropic self-assembly of spherical polymer-grafted nanoparticles. *Nat. Mater.* **2009**, *8*, 354−359.

(5) Akcora, P.; Kumar, S. K.; Moll, J.; Lewis, S.; Schadler, L. S.; Li, Y.; Benicewicz, B. C.; Sandy, A.; Narayanan, S.; Ilavsky, J.; Thiyagarajan, P.; Colby, R. H.; Douglas, J. F. "Gel-like" Mechanical Reinforcement in Polymer Nanocomposite Melts. *Macromolecules* **2010**, *43*, 1003−1010.

(6) Song, Y.; Zheng, Q. Concepts and conflicts in nanoparticles reinforcement to polymers beyond hydrodynamics. *Prog. Mater. Sci.* **2016**, *84*, 1−58.

(7) Mangal, R.; Srivastava, S.; Archer, L. A. Phase stability and dynamics of entangled polymer−nanoparticle composites. *Nat. Commun.* **2015**, *6*, No. 7198.

(8) Kim, D.; Srivastava, S.; Narayanan, S.; Archer, L. A. Polymer nanocomposites: polymer and particle dynamics. *Soft Matter* **2012**, *8*, 10813−10818.

(9) Xia, S.; Liu, X.; Wang, J.; Kan, Z.; Chen, H.; Fu, W.; Li, Z. Role of poly(ethylene glycol) grafted silica nanoparticle shape in toughened PLA-matrix nanocomposites. *Composites, Part B* **2019**, *168*, 398−405.

(10) Wei, T.; Jin, K.; Torkelson, J. M. Isolating the effect of polymer-grafted nanoparticle interactions with matrix polymer from dispersion on composite property enhancement: The example of polypropylene/halloysite nanocomposites. *Polymer* **2019**, *176*, 38−50.

(11) Giovino, M.; Pribyl, J.; Benicewicz, B.; Kumar, S.; Schadler, L. Linear rheology of polymer nanocomposites with polymer-grafted nanoparticles. *Polymer* **2017**, *131*, 104−110.

(12) Maillard, D.; Kumar, S. K.; Fragneaud, B.; Kysar, J. W.; Rungta, A.; Benicewicz, B. C.; Deng, H.; Brinson, L. C.; Douglas, J. F. Mechanical Properties of Thin Glassy Polymer Films Filled with Spherical Polymer-Grafted Nanoparticles. *Nano Lett.* **2012**, *12*, 3909−3914.

(13) Randazzo, K.; Bartkiewicz, M.; Graczykowski, B.; Cangialosi, D.; Fytas, G.; Zuo, B.; Priestley, R. D. Direct Visualization and Characterization of Interfacially Adsorbed Polymer atop Nanoparticles and within Nanocomposites. *Macromolecules* **2021**, *54*, 10224−10234.

(14) Bailey, E. J.; Winey, K. I. Dynamics of polymer segments, polymer chains, and nanoparticles in polymer nanocomposite melts: A review. *Prog. Polym. Sci.* **2020**, *105*, No. 101242.

(15) Mangal, R.; Wen, Y. H.; Choudhury, S.; Archer, L. A. Multiscale Dynamics of Polymers in Particle-Rich Nanocomposites. *Macromolecules* **2016**, *49*, 5202−5212.

(16) You, W.; Yu, W. Slow Linear Viscoelastic Relaxation of Polymer Nanocomposites: Contribution from Confined Diffusion of Nanoparticles. *Macromolecules* **2019**, *52*, 9094−9104.

(17) Senses, E.; Ansar, S. M.; Kitchens, C. L.; Mao, Y.; Narayanan, S.; Natarajan, B.; Faraone, A. Small Particle Driven Chain Disentanglements in Polymer Nanocomposites. *Phys. Rev. Lett.* **2017**, *118*, No. 147801.

(18) Yang, S.; Hassan, M.; Akcora, P. Role of adsorbed chain rigidity in reinforcement of polymer nanocomposites. *J. Polym. Sci., Part B: Polym. Phys.* **2019**, *57*, 9−14.

(19) Salatto, D.; Carrillo, J.-M. Y.; Endoh, M. K.; Taniguchi, T.; Yavitt, B. M.; Masui, T.; Kishimoto, H.; Tyagi, M.; Ribbe, A. E.; Garcia Sakai, V.; Kruteva, M.; Sumpter, B. G.; Farago, B.; Richter, D.; Nagao, M.; Koga, T. Structural and Dynamical Roles of Bound Polymer Chains in Rubber Reinforcement. *Macromolecules* **2021**, *54*, 11032−11046.

(20) Wu, D.; Feng, Y.; Li, R.; Ozisik, R.; Akcora, P. Entanglement density and particle dynamics in rigid interfacial layers of polymer nanocomposites. *J. Appl. Phys.* **2021**, *130*, No. 064701.

(21) Yang, S.; Liu, S.; Narayanan, S.; Zhang, C.; Akcora, P. Chemical heterogeneity in interfacial layers of polymer nanocomposites. *Soft Matter* **2018**, *14*, 4784−4791.

(22) Termonia, Y. Chain confinement in polymer nanocomposites and its effect on polymer bulk properties. *J. Polym. Sci., Part B: Polym. Phys.* **2010**, *48*, 687−692.

(23) Schneider, G. J.; Nusser, K.; Willner, L.; Falus, P.; Richter, D. Dynamics of Entangled Chains in Polymer Nanocomposites. *Macromolecules* **2011**, *44*, 5857−5860.

(24) Crosby, A. J.; Lee, J. Y. Polymer Nanocomposites: The "Nano" Effect on Mechanical Properties. *Polym. Rev.* **2007**, *47*, 217−229.

(25) Rittigstein, P.; Priestley, R. D.; Broadbelt, L. J.; Torkelson, J. M. Model polymer nanocomposites provide an understanding of confinement effects in real nanocomposites. *Nat. Mater.* **2007**, *6*, 278−282.

(26) Senses, E.; Isherwood, A.; Akcora, P. Reversible Thermal Stiffening in Polymer Nanocomposites. *ACS Appl. Mater. Interfaces* **2015**, *7*, 14682−14689.

(27) Wu, D.; Weiblen, D. G.; Ozisik, R.; Akcora, P. Local Viscosity of Interfacial Layers in Polymer Nanocomposites Measured by Magnetic Heating. *ACS Appl. Polym. Mater.* **2020**, *2*, 5542−5549.

(28) Peng, W.; Ranganathan, R.; Keblinski, P.; Akcora, P.; Ozisik, R. Viscoelastic and dynamic properties of polymer grafted nanocomposites with high glass transition temperature graft chains. *J. Appl. Phys.* **2019**, *126*, No. 195102.

(29) Zhong, Y.; Tu, J.; Yu, Y.; Xu, J.; Tan, D. Temperature compensation in viscoelastic damper using magnetorheological effect. *J. Sound Vib.* **2017**, *398*, 39−51.
(30) Lewandowski, R.; Przychodzki, M. Approximate method for temperature-dependent characteristics of structures with viscoelastic dampers. *Arch. Appl. Mech.* **2018**, *88*, 1695−1711.
(31) Kadiyala, A. K.; Bijwe, J. Investigations on performance and failure mechanisms of high temperature thermoplastic polymers as adhesives. *Int. J. Adhes. Adhes.* **2016**, *70*, 90−101.
(32) Haley, J. C.; Lodge, T. P. Dynamics of a poly(ethylene oxide) tracer in a poly(methyl methacrylate) matrix: Remarkable decoupling of local and global motions. *J. Chem. Phys.* **2005**, *122*, No. 234914.
(33) Lutz, T. R.; He, Y.; Ediger, M. D.; Cao, H.; Lin, G.; Jones, A. A. Rapid poly(ethylene oxide) segmental dynamics in blends with poly(methyl methacrylate). *Macromolecules* **2003**, *36*, 1724−1730.
(34) Niedzwiedz, K.; Wischnewski, A.; Monkenbusch, M.; Richter, D.; Genix, A. C.; Arbe, A.; Colmenero, J.; Strauch, M.; Straube, E. Polymer chain dynamics in a random environment: Heterogeneous mobilities. *Phys. Rev. Lett.* **2007**, *98*, No. 168301.
(35) Ito, H.; Russell, T. P.; Wignall, G. D. Interactions in Mixtures of Poly(ethylene oxide) and Poly(methyl methacrylate). *Macromolecules* **1987**, *20*, 2213−2220.
(36) Brodeck, M.; Alvarez, F.; Moreno, A. J.; Colmenero, J.; Richter, D. Chain motion in nonentangled dynamically asymmetric polymer blends: Comparison between atomistic simulations of PEO/PMMA and a generic bead-spring model. *Macromolecules* **2010**, *43*, 3036−3051.
(37) Pedemonte, E.; Polleri, V.; Turturro, A.; Cimmino, S.; Silvestre, C.; Martuscelli, E. Thermodynamics of poly(ethylene oxide)-poly-(methyl methacrylate) blends: prediction of miscibility based on the corresponding-states theory. *Polymer* **1994**, *35*, 3278−3281.
(38) Carrillo, J. Y.; Cheng, S.; Kumar, R.; Goswami, M.; Sokolov, A. P.; Sumpter, B. G. Untangling the Effects of Chain Rigidity on the Structure and Dynamics of Strongly Adsorbed Polymer Melts. *Macromolecules* **2015**, *48*, 4207−4219.
(39) Yang, J.; Melton, M.; Sun, R.; Yang, W.; Cheng, S. Decoupling the polymer dynamics and the nanoparticle network dynamics of polymer nanocomposites through dielectric spectroscopy and rheology. *Macromolecules* **2020**, *53*, 302−311.
(40) Senses, E.; Jiao, Y.; Akcora, P. Modulating interfacial attraction of polymer-grafted nanoparticles in melts under shear. *Soft Matter* **2014**, *10*, 4464−4470.
(41) Senses, E.; Faraone, A.; Akcora, P. Microscopic Chain Motion in Polymer Nanocomposites with Dynamically Asymmetric Interphases. *Sci. Rep.* **2016**, *6*, No. 29326.
(42) Beaucage, G. Small-Angle Scattering from Polymeric Mass Fractals of Arbitrary Mass-Fractal Dimension. *J. Appl. Crystallogr.* **1996**, *29*, 134−146.
(43) Hansoge, N. K.; Gupta, A.; White, H.; Giuntoli, A.; Keten, S. Universal Relation for Effective Interaction between Polymer-Grafted Nanoparticles. *Macromolecules* **2021**, *54*, 3052−3064.
(44) Mardles, E. W. J. Viscosity of Suspensions and the Einstein Equation. *Nature* **1940**, *145*, No. 970.
(45) Fetters, L. J.; Lohse, D. J.; Richter, D.; Witten, T. A.; Zirkel, A. Connection between Polymer Molecular Weight, Density, Chain Dimensions, and Melt Viscoelastic Properties. *Macromolecules* **1994**, *27*, 4639−4647.
(46) Kumar, S. K.; Jimenez, A. M. Polymer adsorption-reversible or irreversible? *Soft Matter* **2020**, *16*, 5346−5347.
(47) Senses, E.; Akcora, P. An Interface-Driven Stiffening Mechanism in Polymer Nanocomposites. *Macromolecules* **2013**, *46*, 1868−1874.

https://doi.org/10.1021/acsapm.2c00097
ACS Appl. Polym. Mater. 2022, 4, 2819−2827